J Mater Sci: Mater Med (2016)27:185
DOI 10.1007/s10856-016-5796-0

ENGINEERING AND NANO-ENGINEERING APPROACHES FOR MEDICAL DEVICES

Original Research

# Increased cellular uptake of lauryl gallate loaded in superparamagnetic poly(methyl methacrylate) nanoparticles due to surface modification with folic acid

**Paulo Emilio Feuser[1] · Juan Marcelo Carpio Arévalo[2] · Enio Lima Junior[3] · Gustavo Rodrigues Rossi[4] · Edvaldo da Silva Trindade[4] · Maria Eliane Merlin Rocha[2] · Amanda Virtuoso Jacques[5] · Eduardo Ricci-Júnior[6] · Maria Claudia Santos-Silva[5] · Claudia Sayer[1] · Pedro H. Hermes de Araújo[1]**

Received: 20 July 2016 / Accepted: 13 October 2016
© Springer Science+Business Media New York 2016

**Abstract** Lauryl gallate loaded in superparamagnetic poly (methyl methacrylate) nanoparticles surface modified with folic acid were synthesized by miniemulsion polymerization in just one step. In vitro biocompatibility and cytotoxicity assays on L929 (murine fibroblast), human red blood, and HeLa (uterine colon cancer) cells were performed. The effect of folic acid at the nanoparticles surface was evaluated through cellular uptake assays in HeLa cells. Results showed that the presence of folic acid did not affect substantially the polymer particle size (~120 nm), the superparamagnetic behavior, the encapsulation efficiency of lauryl gallate (~87 %), the Zeta potential (~38 mV) of the polymeric nanoparticles or the release profile of lauryl gallate. The release profile of lauryl gallate from superparamagnetic poly(methyl methacrylate) nanoparticles presented an initial burst effect (0–1 h) followed by a slow and sustained release, indicating a biphasic release system. Lauryl gallate loaded in superparamagnetic poly(methyl methacrylate) nanoparticles with folic acid did not present cytotoxicity effects on L929 and human red blood cells. However, free lauryl gallate presented significant cytotoxic effects on L929 and human red blood cells at all tested concentrations. The presence of folic acid increased the cytotoxicity of lauryl gallate loaded in nanoparticles on HeLa cells due to a higher cellular uptake when HeLa cells were incubated at 37 °C. On the other hand, when the nanoparticles were incubated at low temperature (4 °C) cellular uptake was not observed, suggesting that the uptake occurred by folate receptor mediated energy-dependent endocytosis. Based on presented results our work suggests that this carrier system can be an excellent alternative in targeted drug delivery by folate receptor.

✉ Pedro H. Hermes de Araújo
pedro.h.araujo@ufsc.br

[1] Department of Chemical Engineering and Food Engineering, Federal University of Santa Catarina, Florianópolis, Brazil

[2] Department of Biochemistry and Molecular Biology, Federal University of Paraná, Curitiba, Brazil

[3] Laboratório de Resonancias Magnéticas, Centro Atómico Bariloche & CONICET, San Carlos de Bariloche, Argentina

[4] Department of Cellular Biology, Federal University of Paraná, Curitiba, Brazil

[5] Department of Clinical Analyses, Federal University of Santa Catarina, Florianópolis, Brazil

[6] Department of Pharmacy, Federal University of Rio Janeiro, Rio de Janeiro, Brazil

Published online: 27 October 2016

**Graphical Abstract**

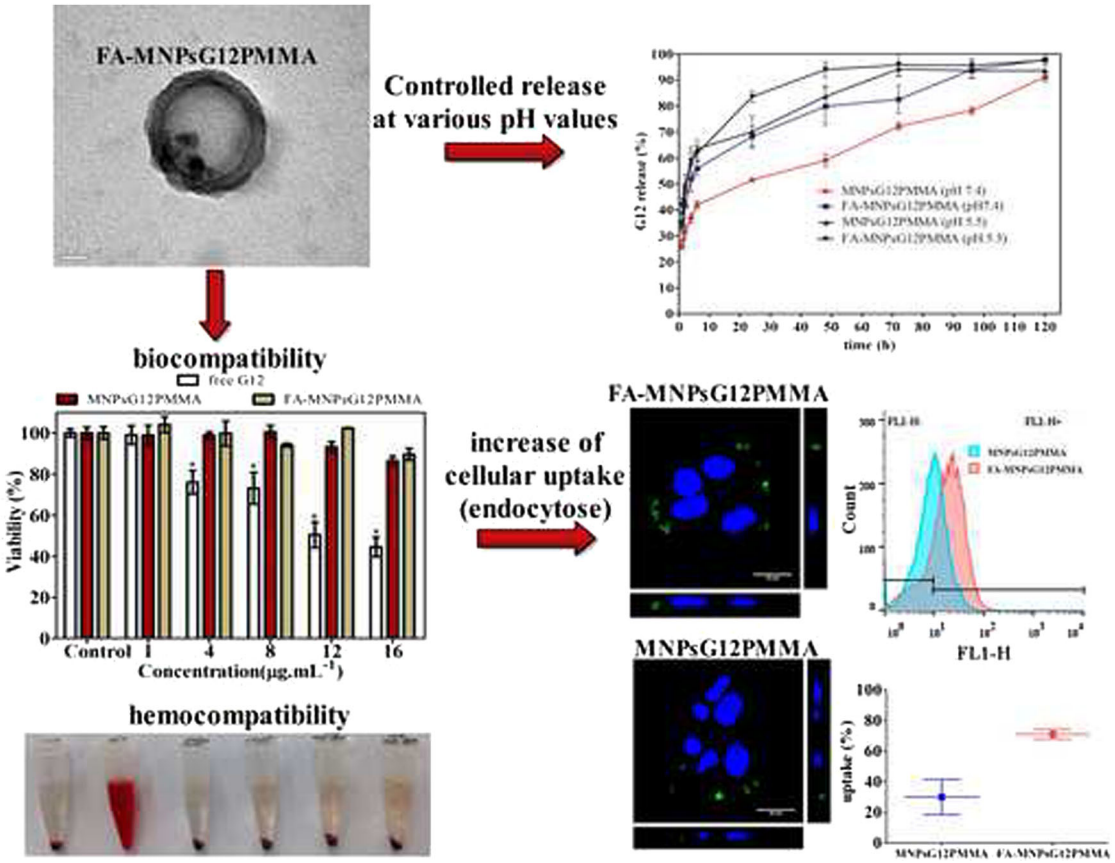


## 1 Introduction

Superparamagnetic polymeric nanoparticles have showed a high potential for various biomedical applications such as drug delivery, controlled drug release, and hyperthermia [1–7]. For these applications, nanoparticles must combine high magnetic saturation, superparamagnetic properties, and biocompatibility [8, 9]. The superparamagnetic behavior is very important for biomedical applications, which, without an external magnetic field their overall magnetization value is randomized to zero, preventing active behavior of the particles when there is no applied field [6, 7, 10], resulting in an excellent strategy to drug delivery [6, 11, 12] and cancer treatment by hyperthermia [4, 9]. Several strategies have been proposed in the literature to encapsulate iron oxide in polymeric nanoparticles being miniemulsion polymerization a very attractive technique for biomedical applications [13] as it allows the incorporation of iron oxide in just one step in different polymerization systems such as step-growth [14] and free radical polymerization [4, 5]. The very flexible nature of miniemulsion polymerization allows the incorporation of several compounds inside the polymeric nanoparticles as well as the surface modification to improve the efficacy of targeted drug delivery [15, 16].

Folic acid (FA) has been used to modify the surface of polymeric nanoparticles increasing the efficiency of *targeted drug delivery* in cancer treatment [17–20] as the folate receptor is significantly overexpressed on the surface of different human cancer cells [16, 18, 19, 21, 22]. Folate receptor-mediated drug delivery is based on conjugation with FA, which promotes drug uptake by folate receptor-mediated endocytosis [21, 23, 24]. The main advantage of using FA as binding agent is their absent expression on non-tumor cells [16, 22]. The encapsulation of anticancer drugs in superparamagnetic polymeric systems can be an excellent strategy in cancer treatment, ensuring selective drug delivery with controlled release and reducing possible toxic effects [6, 11, 25]. Other advantage of the superparamagnetic polymeric systems is the combination of hyperthermia with other cancer treatment methods, such as chemotherapy, that could increase the efficacy of cancer therapy [26].

Gallic acid (GA) is a natural antioxidant, which is obtained from the hydrolysis of natural plant polyphenols [27].

GA and its ester derivatives, such as octyl and lauryl gallate, have been shown to be involved in a wide variety of biological actions. The biological activity of GA and its derivatives has been described in the literature as antimalarial [28], antioxidant [27, 29, 30], anticancer [30, 31], and antibacterial [31]. The difference among the ester derivatives is found in the number of carbon atoms in the aliphatic side chain, giving them different physicochemical characteristics, especially lipophilicity evaluated by the partition coefficient value [27, 32]. These ester derivatives, especially those with eight or more carbon atoms in the side-chain, were more efficient than GA in antiviral, antifungal, antioxidant, and antitumoral activities [32]. Although some of these ester derivatives showed a high cytotoxic activity, the chemical derivatization decreased their water solubility, constituting a disadvantage for intravenous administration [33]. According to Ximenes and collaborators [34], GA and ester derivatives could interact and disrupt the red blood cells membrane. Another disadvantage involving the use of GA and it is derivatives is their poor pharmacokinetic profile (low bioavailability) and toxicity when in vivo administered [35]. Therefore the lauryl gallate loaded in superparamagnetic poly(methyl methacrylate) (PMMA) nanoparticles with FA could be guided by an gradient of magnetic field [6, 10, 22], increasing the site-specific drug delivery (increased bioavailability) and reducing undesirable side effect. Furthermore, magnetic nanoparticles can induce cells death by hyperthermia [4, 10, 36]. In addition, these magnetic polymeric systems can improve intravenous administration, as they can be dispersed in water preventing undesired effects, protect drug against degradation providing an excellent strategy for cancer treatment [9, 36–38].

Aiming to improve site-specific drug delivery and reduce undesirable side effects, lauryl gallate loaded in superparamagnetic PMMA nanoparticles with the surface modified with FA was synthesized by miniemulsion polymerization in just one step. The polymeric nanoparticles were characterized and the release profile of lauryl gallate was determined at 37 °C and different pH (7.4 and 5.5). Lastly, in vitro assays were performed to verify the biocompatibility, cytotoxicity, and cellular uptake (at 4 and 37 °C).

## 2 Experimental section

### 2.1 Materials

For synthesis of magnetic nanoparticles coated with oleic acid (MNPs-OA), the following reagents were used (high purity grade): ferrous sulfate ($FeSO_4{\cdot}4H_2O$), iron (III) chloride hexahydrate ($FeCl_3{\cdot}6H_2O$), ammonium hydroxide (99 %), and oleic acid (OA), all purchased from Vetec, Brazil. For the preparation of polymeric nanoparticles, the following reagents were used: methyl methacrylate (MMA), purchased from Arinos Chemistry, azobisisobutyronitrile (AIBN) and FA purchased from Vetec. Lauryl gallate, 6-coumarin, and N-methylpyrrolidone, purchased from Sigma Aldrich, lecithin purchased from Alpha Aesar, and crodamol purchased from Croda. Distilled water was used throughout the experiments.

### 2.2 Methods

#### *2.2.1 Synthesis of MNPs-OA*

MNPs-OA were prepared by co-precipitation in medium aqueous as described by Feuser and collaborates [4]. Briefly, $FeCl_3.6H_2O$ and $FeSO_4.7H_2O$ (mole ratio of 1:1.2) were dissolved in a beaker containing distilled water under mechanical stirring in the 800 rpm range. Then an ammonium hydroxide solution (11 mL) was rapidly added to the solution. After 1 h, 30 mL was added to the OA and the stirring process continued (800 rpm) for 30 min. The MNPs-OA produced were centrifuged and washed three times with ethanol to remove unreacted OA.

#### *2.2.2 Synthesis of lauryl gallate loaded in superparamagnetic PMMA nanoparticles (MNPsG12PMMA)*

MNPsG12PMMA nanoparticles were prepared by miniemulsion polymerization as described by Feuser and collaborates [5]. Initially 1 mL of N-methylpyrrolidone containing 40 mg of lauryl gallate (lauryl gallate) was added dropwise into a beaker containing 20 mL of distilled water (aqueous phase) under sonication with an amplitude of 70 % (Fisher Scientific, Sonic Dismembrator, 500 W). Then, the organic phase containing 2 g of MMA (monomer) coated 0.4 g of MNPs-OA, 0.1 g of lecithin (surfactant), 0.1 g of crodamol (costabilizer), and 0.04 g of AIBN (initiator) was added dropwise under higher shear to the previous aqueous lauryl gallate dispersion. The sonication was continued for 5 min (10 s on and 1 s off) in a beaker immersed in an ice bath to avoid a temperature increase during sonication. The miniemulsion was transferred to glass tubes (10 mL) at 70 °C, for polymerization during 3 h. Afterwards, the material was cooled, centrifuged, and washed three times with phosphate buffered saline (PBS) at pH 7.4. Subsequently, polymeric nanoparticles were transferred to glass vials, frozen in liquid nitrogen, and lyophilized (FreeZone 4.5-L Benchtop Freeze Dry System; Labconco, Kansas City, MO, USA). The

lyophilized powder was stored at room temperature before analysis.

#### 2.2.3 Synthesis of lauryl gallate (lauryl gallate) loaded in superparamagnetic PMMA nanoparticles surface modified with FA (FA-MNPsG12PMMA)

FA-MNPsG12PMMA nanoparticles were obtained by miniemulsion polymerization. Initially 1 mL of N-methylpyrrolidone containing 40 mg of lauryl gallate was added dropwise into a beaker containing 20 mL of distilled water and 0.002 g of FA (aqueous phase) under sonication with an amplitude of 70 % (Fisher Scientific, Sonic Dismembrator, 500 W). Next, the organic phase containing 2 g of MMA (monomer) coated with 0.4 g of MNPs-OA, 0.1 g of lecithin (surfactant), 0.1 g of crodamol (costabilizer), and 0.04 g of AIBN (initiator) was added dropwise under higher shear to the previous aqueous lauryl gallate dispersion. The next steps were the same as described previously.

### 2.3 Characterization

The superparamagnetic polymeric nanoparticles morphology was observed using a transmission electron microscope (TEM), model JEM 2100F, operating at 100 kV. For TEM analysis, several drops of the diluted sample (1:10) was placed on a 200 mesh Formvar/carbon copper grid (Electron Microscopy Science). After drying, samples were sputter-coated with a thin layer of carbon film to avoid the degradation of the PMMA under the electron beam and observed at 80 kV. Average particle size and polydispersity index (PdI) were also measured by dynamic light scattering and the surface charge of the nanoparticles was investigated through zeta potential measurements (in both cases using the same Zetasizer). All samples were analyzed three times, from which we calculated the average and standard deviation (SD). X-ray diffraction (XRD) experiments were performed to identify the crystallographic structure of the free drug and superparamagnetic polymeric nanoparticles. Fourier transform infrared spectroscopy (FTIR) was used to confirm the chemical structure of the superparamagnetic polymeric nanoparticles using a KBr pellet. Ultraviolet–Visible (UV–Vis) spectrum was performed to verify the FA adsorption in superparamagnetic PMMA nanoparticles. Nanoparticles were measured through TGA runs under a nitrogen atmosphere at a heating rate of 10 °C/min. A Lakeshore vibration sample magnetometer was used to measure the hysteresis loops of MNPs-OA and lauryl gallate loaded in superparamagnetic PMMA nanoparticles surface modified with FA in the temperature range of 300–80 K, while a QUANTUN DESIGNS MPMS-5 SQUID magnetometer was used for the measurements of thermal dependence of magnetization in Field-Cooling (FC) and Zero-Field-Cooling modes (ZFC). For FTIR and TGA analyses the samples were centrifuged (13,400 rpm) and lyophilized (Lyophilizer, FreeZone 4.5-L Benchtop Freeze Dry System Labconco, Kansas City, USA). For magnetization measurements, the lyophilized nanoparticles where dispersed in a polymeric matrix (polyethylenimine) in the concetrations of 2.7 % for lauryl gallate loaded in superparamagnetic PMMA nanoparticles and 6.7 % for MNPs-OA in order to avoid the mechanical rotation of the nanoparticles with the applied field and to reduce the effects of interparticle interactions. The graph was plotted using OriginPro 8 software.

#### 2.3.1 Encapsulation efficiency (EE) of lauryl gallate

The EE(%) of lauryl gallate was analyzed using UV–Vis spectrophotometry [5], where 10 mg of superparamagnetic polymeric nanoparticles were dissolved in N-methylpyrrolidone, the common solvent for both drug and polymer. The determination coefficient ($R^2$) exceeded 0.997, with excellent linearity. The lauryl gallate concentration was measured at 273 nm (ultraviolet region of the electromagnetic spectrum) using a calibration curve with different concentrations of lauryl gallate (0.2–2 μg/mL) dispersed in N-methylpyrrolidone. The EE(%) of lauryl gallate was calculated from Equation (1):

$$EE(\%) = \frac{M_1}{M_t} \times 100 \quad (1)$$

where EE is the lauryl gallate encapsulation efficiency, $M_1$ is the mass of lauryl gallate in nanoparticles, and $M_t$ is the mass of lauryl gallate used in formulation. The experiments were run in triplicate ($n = 3$).

#### 2.3.2 Controlled and kinetic release

The release was carried out in the diffusion cell. Superparamagnetic polymeric nanoparticles (15 mg) were weighed and placed in the donor compartment of the diffusion cell. A cellulose acetate membrane (cellulose membrane tubing dialysis, Follow-Aldrich, Ref D9652-100TF) was used for separating donor compartments containing the nanoparticles of the receptor compartment that contained 20 mL of PBS (pH 7.4) with 0.5 % Sodium dodecyl sulfate (SDS) or PBS (pH 5.5) with 0.5 % SDS. A release study with acidic medium receptor (PBS pH 5.5 with 0.5 % SDS) was carried out to simulate the medium lysosomal of tumor cells. The membrane is thin and porous allowing free diffusion of the solvent and drug. Receptor medium was continuously stirred (100 rpm) and the temperature was maintained at 37 °C in a thermostatically controlled water bath. The release studies

followed the sink conditions. At 1, 2, 4, 6, 24, 48, 72, 96, and 120 h, an aliquot was withdrawn from the receptor medium of the release studies. The release study was performed in triplicate ($n = 3$). The drug released in the receptor medium was quantified by spectrophotometry using the visible region of the spectrum (273 nm). The analytical curve was made in the concentration range from 1.6 to 8.8 μg/mL with a determination coefficient of 0.999. The release profile was obtained by associating the percentage of drug released with time. The release data were fitted using the mathematical models of zero order ($Qt = Q_0 + K_0t$), first order ($\ln Qt = \ln Q_0 + K_1t$) and Higuchi ($Qt = K_Ht^{1/2}$) described by Costa and Lobo [39], and the determination coefficient ($R^2$) and straight line equation were determined using the software Excel. The mathematical model with best fit is the model that provides the highest value of determination coefficient. The graph was plotted using OriginPro 8 software.

### 2.3.3 Biocompatibility assay on L929 (murine fibroblast) cells

The L929 cell lines were selected to evaluate cytotoxicity as a direct contact test, as recommended by ISO 10993 [40] for in vitro toxicity. The cells were cultured in Dulbecco's Modified Eagle's medium supplemented with 10 % fetal bovine serum, penicillin (100 units/mL), streptomycin (100 mg/mL), and 4 mM/L of glutamine at 37 °C in tissue culture flasks with 5 % $CO_2$. For experimental purposes, trypsinized cells were adjusted to a concentration of $1 \times 10^4$ cells/well and plated in a 96-well flat bottom culture plate. After 24 h, the cells were treated with a medium containing free lauryl gallate (dissolved in dimethyl sulfoxide (DMSO)), lauryl gallate loaded in superparamagnetic PMMA nanoparticles with or without FA (dissolved in PBS 7.4) at five concentrations: 1, 4, 8, 12, and 16 μg/mL (all assays were performed at equivalent lauryl gallate concentrations) (5 % $CO_2$, 37 °C). After of incubation time (24 h) the free lauryl gallate and nanoparticles were washed three times with PBS and cell viability was assessed using the classical (3-(4,5-Dimethylthiazol-2-yl)-2,5-Diphenyltetrazolium Bromide) (MTT) assay (Sigma, MO, USA).

### 2.3.4 In vitro cytotoxicity assay on HeLa (human cervical cancer cells) cells

HeLa cell lines were obtained from the Adolfo Lutz Institute (São Paulo). HeLa cells were grown in MEM medium containing 7.5 % fetal bovine serum and maintained at 37 °C in a humidified incubator containing 5 % $CO_2$. The HeLa cells were seeded at $1 \times 10^4$ cells/well in 96-well plate. After 24 h, the cells were treated with a medium containing free lauryl gallate (dissolved in DMSO), lauryl gallate loaded in superparamagnetic PMMA nanoparticles with or without FA (dissolved in PBS 7.4) at five concentrations: 10, 11, 12, 13, and 14 μg/mL (all assays were performed at equivalent lauryl gallate concentrations). After 24 h of incubation the cells were washed three times with PBS (7.4) and the MTT cell viability assay was performed. The cytotoxicity assay was carried out in triplicate with three wells for each condition.

### 2.3.5 MTT viability assay

The MTT cell proliferation assay was employed to assess cell viability after both the cytotoxic assays. Briefly, 200 μl aliquots of MTT solution (5 mg/mL) were added to each well and incubated for 3 h (37 °C and 5 % $CO_2$), to allow the formazan-formation reaction. Following incubation, the medium containing the MTT solution was removed, and the formazan crystals were dissolved in DMSO. The absorbance was measured at 550 nm using an Infinite 200 TECAN microplate reader. The results are presented as survival percentage (100 %), where the control group contained 0.1 % DMSO (v/v).

### 2.3.6 Hemolysis assay

This study was approved by the medical ethics committee of Polydoro Ernani de São Thiago University Hospital (Florianopolis, Brazil) as described previously [17]. Citrate-stabilized human blood was freshly collected and used within 3 h of being drawn. 4 mL of whole blood was added to 8 mL of a sterile solution of sodium chloride in water (saline) and the human red blood cells were isolated from serum by centrifugation at $10{,}000 \times g$ for 5 min. The human red blood cells were further washed five times with saline solution. Following the last wash, the human red blood cells were diluted in 2 mL of saline solution and then 120 μL of the diluted human red blood cells suspension was added to 880 μL of water or saline. The free lauryl gallate dissolved in DMSO (0.1 %), lauryl gallate loaded in superparamagnetic PMMA nanoparticles surface modified with FA dissolved in PBS (pH 7.4) were treated at concentrations 10, 25, and 50 μg/mL (all assays were performed at equivalent lauryl gallate concentrations). All samples were prepared in triplicate and the suspension was briefly vortexed before gentle stirring at 37 °C for 60 min. After that, the mixture was briefly vortexed again and centrifuged at $10{,}000 \times g$ for 5 min. 100 μL of supernatant from the sample tube was transferred to a 96-well plate. The absorbance value of hemoglobin at 570 nm was measured with the reference wavelength at 540 nm. The 120 μL of diluted red blood cells suspension incubated with 880 μL of water and saline was used as the positive and negative control, respectively. The hemolysis percentage (%) was calculated

using Equation (2):

$$\text{Hemolysis}(\%) = \frac{(\text{sample absorbance} - \text{negative control})}{(\text{positive control} - \text{negative control})} \times 100\% \quad (2)$$

*2.3.7 Cellular uptake assay by laser scanning confocal microscopy*

The internalization of carrier systems labeled with 6-coumarin (MNPsG12PMMA and FA-MNPsG12PMMA) were evaluated with laser scanning confocal microscopy. HeLa cells ($5 \times 10^4$) were cultured on 13 mm diameter glass coverslips in 24 well plates for 72 h. Cells were then treated with 10 µg/mL (lauryl gallate concentration) of lauryl gallate loaded in superparamagnetic PMMA nanoparticles labeled with 6-coumarin [17] with and without FA (in PBS), and incubated for 1 h, at 37 °C. In order to block the endocytotic (energy-dependent) pathways of lauryl gallate loaded in superparamagnetic PMMA nanoparticles with or without FA (dissolved in PBS) were also incubated for 1 h at 4 °C. After the incubation, cells were washed with PBS (three times), fixed with 2 % paraformaldehyde (Electron Microscopy Science) in PBS, for 20 min at 22 °C. Coverslips were then mounted using Prolong Gold with nuclear stain DAPI (4′,6-diamidino-2-phenylindole) (Thermo Fisher) and examined by laser scanning confocal microscopy A1RSi+MP (Nikon Corp, Tokyo, Japan). Fluorescence imaging was acquired exciting 6-coumarin using laser 488 nm and emission was captured using filter 515/30 (500–530 nm bandpass). DAPI was excited with laser 405 nm and the emission was captured using filter 450/50 (425–475 nm bandpass). Cells were observed by DIC (differential interference contrast) image (using the illumination with laser 488 nm and capture of images in transmitted light detector). The resulting images were analyzed using Fiji software.

*2.3.8 Cellular uptake assay by flow cytometry*

HeLa cells ($10^3$) were cultured in 12 well plates for 24 h. Cells were then treated with 10 µg/mL of lauryl gallate loaded in superparamagnetic PMMA nanoparticles surface modified with and without FA, both labeled with 6-coumarin and incubated for 1 h, at 37 °C. As fluorescence control, HeLa cells were incubated without superparamagnetic PMMA nanoparticles. After incubation, the cells were harvested by trypsinization and washed with PBS (three times). Cellular uptake efficacy was evaluated by flow cytometry using a BD FACScalibur cytometer (Becton Dickinson and Company, San Diego, CA, USA). 6-coumarin was excited with laser 488 nm and the emission captured at FL-1H channel (530/30). The results were analyzed using Flowing software 2.

*2.3.9 Statistical analysis*

Data are presented as the mean ± SD of three determinations performed in triplicate. One-way ANOVA followed by the Tukey's test as a post hoc comparison. Statistical analysis was performed using GraphPad Prism v. 5.04 computer program (GraphPad Software, Inc. CA, USA). The statistical significance level was set at $P < 0.05$ for all analysis.

## 3 Results

### 3.1 Characterization of lauryl gallate loaded in superparamagnetic PMMA nanoparticles

Lauryl gallate loaded in superparamagnetic PMMA nanoparticles surface modified with FA were obtained by miniemulsion polymerization with a EE(%) of approximately 87 ± 4 %. TEM analysis (Figs. 1b, d) showed that the incorporation of lauryl gallate and MNPs-OA did not affect the morphology of nanoparticles. The nanoparticles without FA and surface modified with FA presented spherical morphology and a mean size of 100 nm, approximately. Some darker

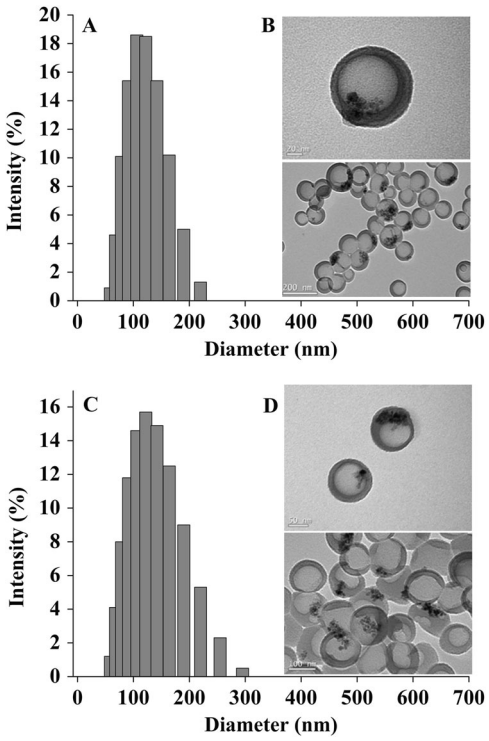


**Fig. 1** Particle size distribution obtained by dynamic light scattering: lauryl gallate loaded in superparamagnetic PMMA nanoparticles with (**a**) and without FA (**c**). TEM images lauryl gallate loaded in superparamagnetic PMMA nanoparticles with (**b**) and without FA (**d**)

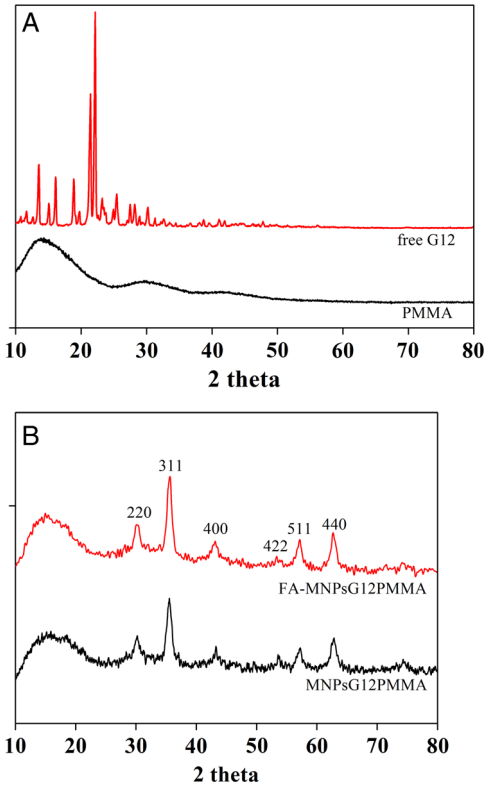


**Fig. 2** X-ray powder diffraction patterns of free lauryl gallate, PMMA, and lauryl gallate loaded in superparamagnetic PMMA nanoparticles with and without FA

regions of very small size, around 5–14 nm in diameter are attributed to the core formed by iron oxide, as can be observed in Figs. 1b and d [41].

Dynamic light scattering analysis (Figs. 1a, c) showed that the superparamagnetic polymeric nanoparticles with and without FA have intensity average particle diameters of $125 \pm 4$ nm and $106 \pm 3$ nm and a PdI of $0.19 \pm 0.03$ and $0.15 \pm 0.02$, respectively. FA adsorption on the superparamagnetic PMMA nanoparticles increased the average size by approximately 19 nm, when compared to nanoparticles without FA. The zeta potential of nanoparticles with (-38 mV ± 5) and without FA (-40 mV ± 4) did not present significant difference.

The XRD patterns of free lauryl gallate and lauryl gallate loaded in superparamagnetic PMMA nanoparticles with and without FA are shown in Fig. 2. The XRD profile of free lauryl gallate exhibited several characteristic peaks, confirming the crystalline form of lauryl gallate [42]. However, these peaks were not observed in the diffractograms when the lauryl gallate was encapsulated in superparamagnetic PMMA nanoparticles. The peaks observed at 2θ: (220), (311), (400), (422), (511), and (440) are characteristic of iron oxide encapsulated in PMMA nanoparticles [4, 17].

FTIR analyses were performed to verify the incorporation of lauryl gallate and MNPs-OA in the PMMA

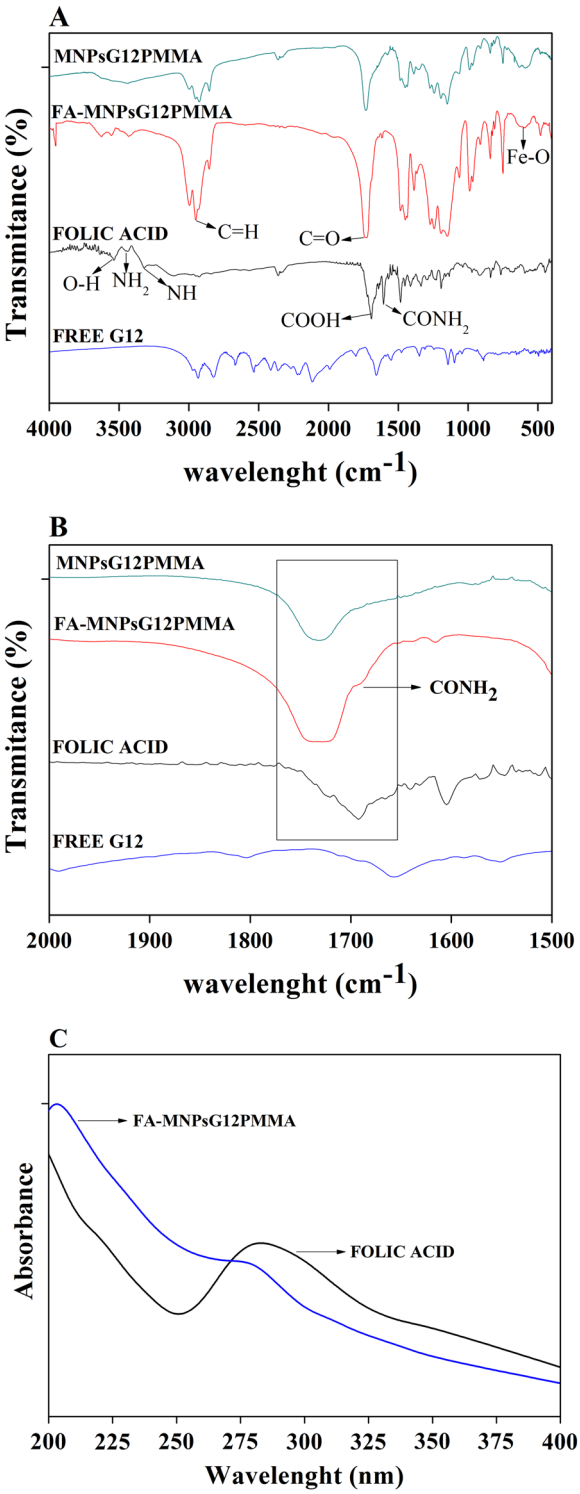


**Fig. 3** FTIR spectrum of free lauryl gallate, FA, and lauryl gallate loaded in superparamagnetic PMMA nanoparticles with FA and without FA (**a** and **b**) and UV–Vis spectrum of FA adsorbed on superparamagnetic PMMA nanoparticles (**c**)

nanoparticles. In addition, the FTIR technique can indicate FA adsorption on nanoparticles. In Fig. 3a, the peaks at 1736 $cm^{-1}$ and 3000–2800 $cm^{-1}$ correspond to C=O groups

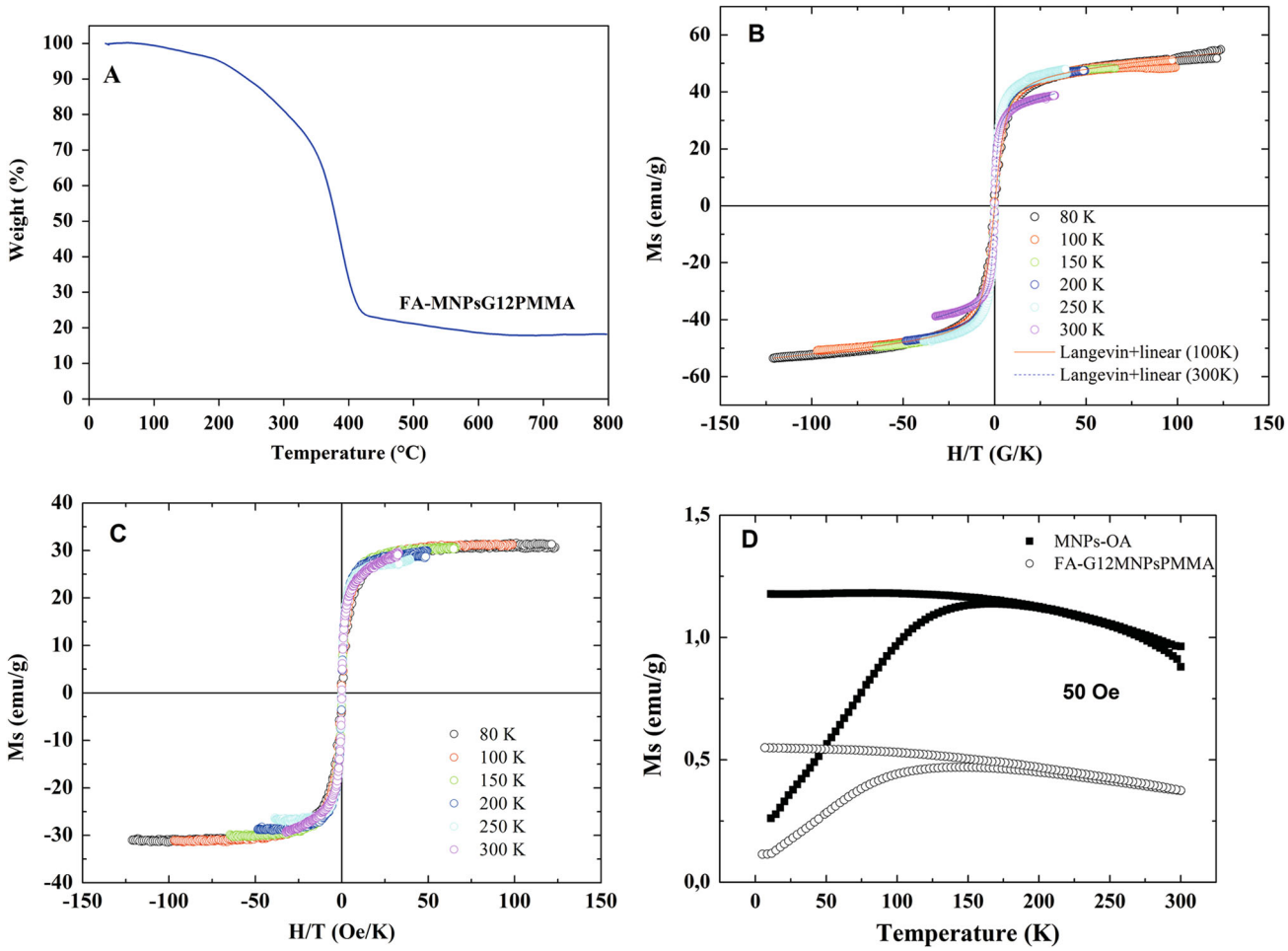


**Fig. 4** TGA analysis of lauryl gallate loaded in superparamagnetic PMMA nanoparticles with FA (**a**). Magnetization curves plotted as M vs. H/T (Langevin plot) of MNPs-OA (**b**) and lauryl gallate loaded in superparamagnetic PMMA nanoparticles surface modified with FA (**c**). ZFC–FC curves of MNPs-OA and lauryl gallate loaded in superparamagnetic PMMA nanoparticles surface modified with FA (**d**)

and stretching of C–H bonds, characteristic of PMMA nanoparticles [5]. The peak at 577 $cm^{-1}$ is related to the vibration of the Fe–O bond, which matches well with the characteristic peak of iron oxide [14, 19, 43]. FTIR spectrum of FA presented peaks at 1680, 1590, 3540, 3423, and 3315 $cm^{-1}$ corresponding to amide I, amide II, ring O–H, $NH_2$, and secondary $NH_2$ groups [20, 23]. The appearance of bands at 3400 $cm^{-1}$ and 1688 $cm^{-1}$ as can be seen in Fig. 3b (small scale), can be indicative of FA adsorption. It is worth mentioning that the superparamagnetic PMMA nanoparticles without FA (Fig. 3b) did not present bands at 1688 $cm^{-1}$. To confirm these results a UV spectrum (Fig. 3c) was performed.

TGA analyses (Fig. 4a) were performed to determine the total concentration of iron oxide in the formulation [43]. The total concentration of iron oxide obtained by the co-precipitation method was 55 %, as described by Feuser and collaborates [4]. In the case of lauryl gallate loaded in superparamagnetic PMMA nanoparticles surface modified with FA the mass loss is gradual and it can be clearly observed that the polymer is completely degraded when reaching a temperature about 430 °C [4, 5, 17].

Figures 4b and c show the Langevin plot (M vs. H/T) for samples MNPs-OA and lauryl gallate loaded in superparamagnetic PMMA nanoparticles surface modified with FA, respectively. First, lauryl gallate loaded in superparamagnetic PMMA nanoparticles presents saturation magnetization (Ms) values of 35 emu/g. This sample also exhibits the superparamagnetic behavior in the entire temperature range studied, reflected as the superposition of all curves. From the Langevin fit, we obtain a moment value of the whole particle that indicates a higher magnetization than the measured (about 60 emu/g), indicating that the real magnetic mass must be considered. Interestingly, the MNPs-OA present a distinct behavior: first, we did not observe the saturation, with a linear contribution at high field; second, we observe only the superposition of the magnetization curves up to 250 K, and for 300 K

**Table 1** Magnetic properties of MNPs-OA and lauryl gallate loaded in superparamagnetic PMMA nanoparticles with and without FA

| Samples | Ms (emu/g) | Mr (emu/g) | Hc (Oe) | Mr/Ms |
|---|---|---|---|---|
| MNPs-OA | 62 | $2.0 \times 10^{-4}$ | 0.5 | $1.7 \times 10^{-5}$ |
| FA-MNPsG12PMMA | 38 | $7.8 \times 10^{-5}$ | 0.1 | $2.0 \times 10^{-5}$ |

a reduction of the magnetic moment is verified. Figure 4d presents the ZFC–FC curves for both samples, indicating for sample of lauryl gallate loaded in superparamagnetic PMMA nanoparticles surface modified with FA an energy barrier distribution expected for blocked-superparamagnetic regime (with mean blocking temperature around 15 K from obtained from the plot of $(1/T)d(M_{ZFC}-M_{FC})/dT$ vs. T, corresponding to an anisotropy energy of $5 \times 10^{-12}$ erg, and a temperature of irreversibility of 150 K, corresponding to the higher blocking temperature present in the system). For sample MNPs-OA, blocking-superparamagnetic regime is also observed.

As expected from the superparamagnetic behavior of lauryl gallate loaded in superparamagnetic PMMA nanoparticles, a low remanent magnetization (Mr)/Ms ratio and a small coercive field (Hc) values are observed for this sample, as shown in Table 1. Similar values are observed for MNPs-OA system, despite it presents a more complex magnetic behavior.

### 3.2 Release kinetics of lauryl gallate from FA-superparamagnetic PMMA nanoparticles

A release study was performed at different pH (7.4 and 5.5), in order to evaluate the release profile of lauryl gallate loaded in superparamagnetic PMMA nanoparticles. The release profiles of lauryl gallate in pH 7.4 and 5.5 exhibited initial burst effect. From 1 h, in both samples and pH conditions, it was observed a slow and sustained release (Fig. 5), following a biphasic release profile. In the range 1–8 h, release occurred at higher speed than in the range of 8–120 h. The release of lauryl gallate from superparamagnetic PMMA nanoparticles was more accelerated in pH 5.5 than pH 7.4. Results also showed that lauryl gallate was released more quickly of superparamagnetic PMMA nanoparticles without FA (Fig. 5).

The zero order, first order and Higuchi mathematical models were used in this study to evaluate the release kinetics. Mathematical models were applied to the release data. The choice of model was based on the highest coefficient of determination ($R^2$). The kinetics of release at physiological and lysosomal pH conditions was best explained by Higuchi model followed by the zero-order model and finally the first order model (Table 2). The release profile showed that lauryl gallate flux is constant and it was released almost immediately from superparamagnetic PMMA nanoparticles with a high lag time (time required for initial drug release), as can be seen in the Table 2.

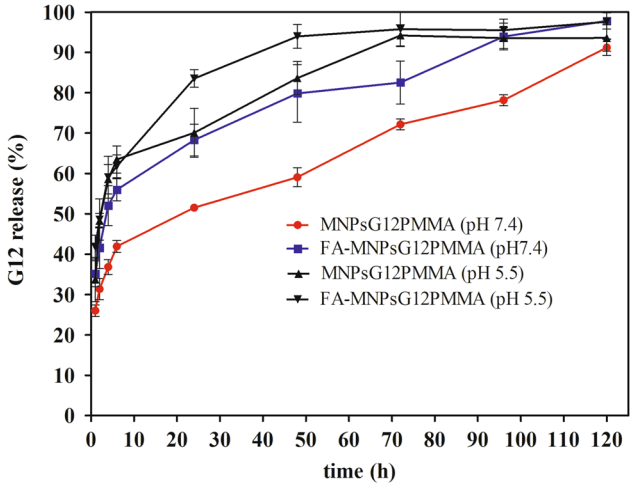


**Fig. 5** Release profiles of lauryl gallate loaded in superparamagnetic PMMA nanoparticles with and without FA at 37 °C and different pH (pH 7.4 and 5.5). Data refers to mean ± SD ($n = 3$). Statistical analysis was performed using one-way ANOVA followed by Tukey's test

### 3.3 In vitro cytotoxicity in L929 and red blood cells assays

In this study the biocompatibility of free lauryl gallate and lauryl gallate loaded in superparamagnetic PMMA nanoparticles was evaluated in L929 cells. Mouse fibroblast (L929) is a popular cell line recommended by ISO 10993-5 [40] for polymer cytotoxicity testing. As shown in Fig. 6a, free lauryl gallate significantly inhibited the L929 cells growth in a dose-dependent manner. However, when the lauryl gallate was encapsulated in superparamagnetic PMMA nanoparticles it was not observed any cytotoxic effects in L929.

The hemolysis assay is another important test for assessment of cytotoxicity on the red blood cells [24, 44]. According to the criterion of Standard Test Method for Analysis of Hemolytic Properties of Nanoparticles (ASTM E2524-08), a percentage hemolysis >5 % indicates that the tested material causes damage. Hemolysis assays of free lauryl gallate showed a high hemolytic percentage at all tested concentrations. The hemolytic percentage reached 16, 25, 33, and 99 % when the human red blood cells were treated with 10, 20, 40, and 80 μ/mL, respectively. On the other hand, the lauryl gallate loaded in superparamagnetic

**Table 2** Mathematical models and kinetic parameters

| Mathematical models | $R^2$ pH 7.4 | $R^2$ pH 5.5 | Flux pH 7.4 | Flux pH 5.5 | Lag time pH 7.4 | Lag time pH 5.5 |
|---|---|---|---|---|---|---|
| MNPsG12PMMA | | | | | | |
| Zero order | 0.960 | 0.774 | 0.490 | 0.427 | 33.963 h | 57.552 h |
| First order | 0.876 | 0.662 | 0.004 | 0.662 | 1.538 h | 1.745 h |
| Higuchi | 0.981 | 0.894 | 5.820 | 5.395 | 23.252 $h^{1/2}$ | 45.884 $h^{1/2}$ |
| FA-MNPsG12PMMA | | | | | | |
| Zero order | 0.884 | 0.739 | 0.471 | 0.428 | 47.945 h | 53.313 h |
| First order | 0.789 | 0.680 | 0.003 | 0.003 | 1.677 h | 1.715 h |
| Higuchi | 0.985 | 0.905 | 5.789 | 5.520 | 36.646 $h^{1/2}$ | 42.287 $h^{1/2}$ |

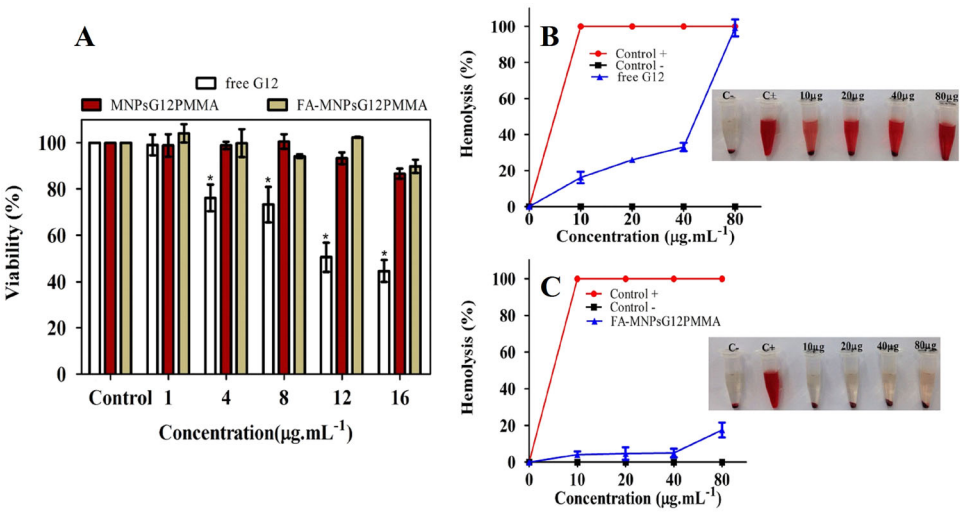


**Fig. 6** Cytotoxicity assays of free lauryl gallate, lauryl gallate loaded in superparamagnetic PMMA nanoparticles with and without FA were performed in L929 cells at different concentrations (**a**). Hemolysis assay (**b** and **c**). Relative rate of hemolysis in human red blood cells upon incubation with free lauryl gallate and FA-MNPslauryl gallatePMMA at different concentrations. Data represent mean ± SD ($n = 3$). (*$P < 0.05$) one-way ANOVA followed by Tukey's test

PMMA nanoparticles surface modified with FA did not exceed 5 % at concentrations of 10 μg/mL (3.5 %), 20 μg/mL (4.2 %), and 40 μg/mL (4.8 %) of lauryl gallate. When the human red blood cells were exposed to a high concentration (80 μg/mL) a small percentage (17 %) was hemolyzed.

### 3.4 In vitro cytotoxicity of lauryl gallate in HeLa cells

The cytotoxic effects of free lauryl gallate and lauryl gallate loaded in superparamagnetic PMMA nanoparticles with and without FA were evaluated in HeLa cells and observed through MTT assay. The aim of this study was to compare the cytotoxic effects of free lauryl gallate and lauryl gallate loaded in superparamagnetic PMMA nanoparticles with and without FA. As can be seen in Fig. 7 the free lauryl gallate did not present any cytotoxic effects on HeLa cells at concentrations of 10 and 11 μg/mL. Lauryl gallate loaded in superparamagnetic PMMA nanoparticles without FA, induced a decrease in cells viability (19 %) at concentration of 11 μg/mL. The cytotoxic effect at concentrations of 10 and 11 μg/mL was more pronounced in lauryl gallate loaded

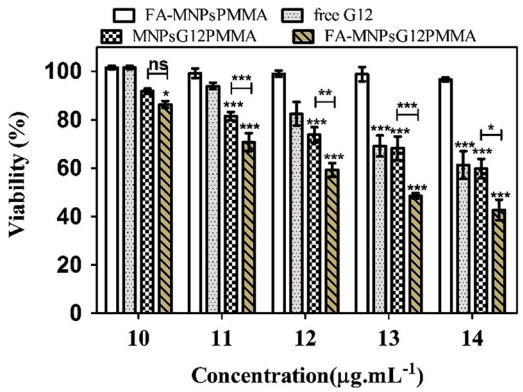


**Fig. 7** In vitro cytotoxicity of free lauryl gallate, lauryl gallate loaded in superparamagnetic PMMA nanoparticles surface modified with and without FA at different concentrations. Data represent three independent experiments, each being performed in triplicate. Significant differences: ***$P < 0.0001$, **$P < 0.0001$, and *$P < 0.0001$ one-way ANOVA followed by Tukey's test

in superparamagnetic PMMA nanoparticles surface modified with FA, which promoted significant reduction in cell viability, 14 and 30 %, respectively. The free lauryl gallate

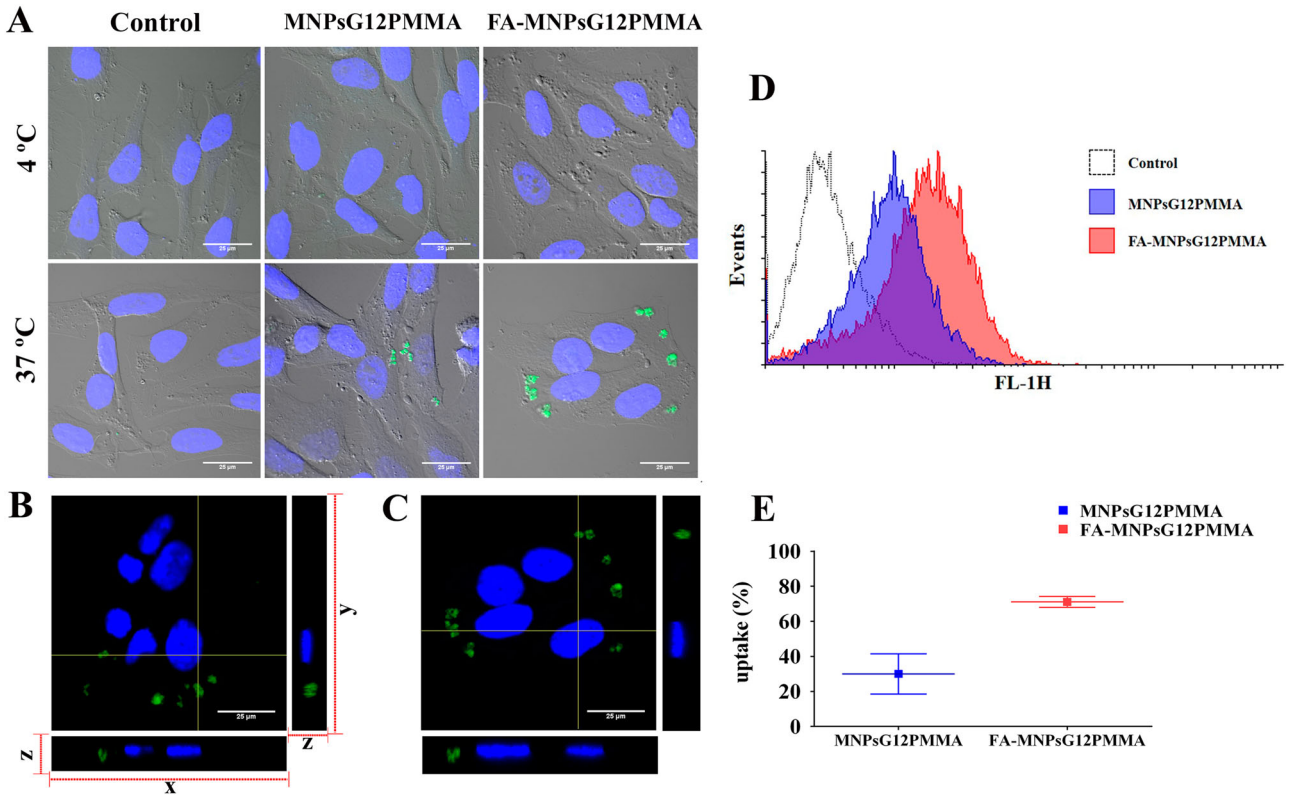


**Fig. 8** Cellular uptake of lauryl gallate loaded in superparamagnetic PMMA nanoparticles (**a**). Cells were incubated for 1 h at 4 °C or 37 °C. Orthogonal view of cells incubated at 37 °C with lauryl gallate loaded in superparamagnetic PMMA nanoparticles surface modified with (**b**) and without FA (**c**). Observe the nuclei in blue (DAPI) and the nanoparticles in green. Histogram of fluorescence (**d**) and quantification (%) (**e**)

induced cell death at concentration range of 12–14 µg/mL, with a decrease in cell viability of 18–39 %, respectively. However, higher cytotoxic effects were observed when HeLa cells were incubated with lauryl gallate loaded in superparamagnetic PMMA nanoparticles surface modified with FA at concentrations range of 12–14 µg/mL decreasing the cell viability of 40–60 %, respectively.

### 3.5 Cellular uptake study by confocal microscopy

To evaluate nanoparticles cellular uptake, HeLa cells were incubated with superparamagnetic PMMA nanoparticles loaded with lauryl gallate with or without surface modified with FA and labeled with 6-coumarin at two different temperatures. Figure 8a shows images of confocal scanning microscopy, at maximum projection of optical slices and merged with DIC.

Superparamagnetic PMMA nanoparticles (green label) incubated at 4 °C cannot be observed inside the cells in Fig. 8a. Note that the nuclei are labeled in blue (with DAPI) and the cells are observed by DIC. When superparamagnetic PMMA nanoparticles were incubated for 1 h at 37 °C, it was observed cellular uptake of both superparamagnetic PMMA nanoparticles (labeled in green) as can be seen in Fig. 8a. To confirm that the nanoparticles were actually internalized and not just bounded to cell surface membrane, an optical slice, containing the nuclei region (labeled with DAPI, blue) was evaluated (Figs. 8b, c). It is clear that the nanoparticles (labeled with 6-coumarin, green) and the nuclei are at the same plan. To reinforce these data, Figs. 8b and c show also an orthogonal view (2D representation of a 3D image). Optical sections xy-projections (inferior panel) and yz-projections (right panel) show the internalized nanoparticles, as they appear at the same plane as the nuclei. Quantification of nanoparticles inside HeLa cells was held by flow cytometry assays. The fluorescence intensity (Fig. 8d) and its corresponding uptake percentage (Fig. 8e) corroborated with confocal microscopy analysis.

## 4 Discussion

Lauryl gallate loaded in superparamagnetic PMMA nanoparticles surface modified with FA were successfully obtained by miniemulsion polymerization with a high EE(%), narrow particle size distribution and spherical morphology, which are considered important parameters for biomedical application

[36, 45]. The high negative zeta potential contributes to an excellent colloidal stability of superparamagnetic PMMA nanoparticles [45]. The negative surface charge of nanoparticles can be attributed to the carboxylic groups (OA and PMMA) and the surfactant (lecithin) on the superparamagnetic PMMA nanoparticles surface [4].

The XRD analysis (Fig. 2) showed that the lauryl gallate is molecularly dispersed in the polymeric matrix in its amorphous state [5, 35, 36], as can be observed at an angle between 10° and 20°, characteristic of an amorphous polymer [46]. Additionally, six peaks, characteristic of iron oxide [4, 17], were observed in the diffractogram of lauryl gallate loaded in superparamagnetic PMMA nanoparticles without FA and surface modified with FA.

FTIR analysis of lauryl gallate loaded in superparamagnetic PMMA nanoparticles confirmed that there was not significant interaction between lauryl gallate and polymer, indicating that the lauryl gallate was embedded into a polymeric matrix. Additionally, the peak at 577 $cm^{-1}$ confirmed the encapsulation of iron oxide. These results were corroborated by XRD analyses. The appearance of two bands (Fig. 3b) characteristic of FA can be indicative of FA adsorption on the nanoparticles surface, due to the interaction of hydrogen bonds [47, 48]. The UV spectrum, as shown in Fig. 3c, confirmed the FA adsorption with the appearance of the band at 284 nm [7, 47, 49].

TGA analysis determined the total concentration of polymer, OA and iron oxide in formulation. The presence of two peaks at around 200 and 440 °C (40 %) are attributed to the OA (different species) on the surface of iron oxide [4, 50]. The residual concentration of approximately 19 %, corresponds to the iron oxide and the others 81 % corresponds to the PMMA and OA adsorbed on the surface of iron oxide [50].

The lauryl gallate loaded in superparamagnetic PMMA nanoparticles surface modified with FA presented superparamagnetic behavior and a Ms value lower than the bulks values of iron oxide (90–100 emu/g of $Fe_3O_4$ and 60–80 emu/g of maghemite ($\gamma$-$Fe_2O_3$)), which is probably related to the encapsulation of the MNPs [4, 50].

Interestingly, the MNPs-OA presented a distinct behavior with a linear contribution at high field. However, it was only observed the superposition of the magnetization curves up to 250 and 300 K. These results indicate that a more complex magnetic order was verified for these nanoparticles in comparison to the first ones: the MNPs-OA system could be seen as a major magnetic monodomain (with superparamagnetic behavior at higher temperatures) with important contributions of surface effects and interparticle interactions. Probably, this sample presented a lower crystallinity degree and/or stronger surface effects [51]. The higher magnetization verified in the curves of the later sample is probably related with a lower amount of organic mass, reducing its effect in the normalized value of magnetization. The ZFC–FC curves, as can be seen in Fig. 4d, evidences that the energy barrier distribution is not well defined, similarly to systems with high surface effects and magnetic disorder even at low temperatures [51, 52], and reinforcing the results obtained from magnetization curves. As expected, the nanoparticles and MNPs-OA presented a low Mr/Ms and small Hc typical of a superparamengnetic behavior (Table 1). It is important to mention that the FA adsorbed and the encapsulation of lauryl gallate in PMMA nanoparticles did not affect the Ms values and magnetic behavior [4, 17].

### 4.1 Controlled release and mathematical models

The release studies of lauryl gallate from supermaparamagnetic PMMA nanoparticles in physiological (7.4) and lysosomal (5.5) pH conditions [19, 52], presented a biphasic release profile, with an initial burst effect following a slow and sustained released, as can be seen in Fig. 5. This biphasic pattern can be attributed to a distribution difference of lauryl gallate entrapped within the polymeric matrix. There is, possibly, a greater amount of drug encapsulated in the surface layer than in the inner portion of the polymer matrix. The biphasic pattern can be an excellent strategy in the development of targeted drug systems, where the drug is released during two periods: (I) immediate drug release to maintain the constant drug concentration in the blood plasma for a prolonged period, followed by a slow and sustained release in the target tissue, consequently improving patient compliance (decreases the number of daily administrations) and therapeutic efficacy [53–56].

Based on the studies of mathematical models shown in Table 2, the release kinetics was best explained by Higuchi model. The Higuchi model describes the drug release from a solid matrix by diffusion based on Fick's law [39, 46]. Generally, diffusion is the mechanism that controls the drug release in delivery systems produced with non-biodegradable polymers, such as PMMA and consequently factors, such as concentration gradient, location of the drug in the polymer matrix, diffusion distance, and the degree of swelling can influence the profile and the release rate [56–58]. Thus, we can conclude that the release of lauryl gallate from the superparamagnetic PMMA nanoparticles followed the Higuchi model and the mechanism that controls the release is the diffusion.

### 4.2 In vitro cytotoxicity in L929 and red blood cells

Lauryl gallate loaded in superparamagnetic PMMA nanoparticles without FA and surface modified with FA did not present any cytotoxic effect on L929 and red blood cells, whereas free lauryl gallate demonstrated cytotoxicity on

L929 and red blood cells as already observed in other studies with free GA derivatives [32, 59]. These results indicate that PMMA nanoparticles provided a drug protection decreasing its cytotoxic effects [36, 38]. In hemolysis assays (Figs. 6b, c) the lauryl gallate encapsulated in superparamagnetic PMMA nanoparticles surface modified with FA did not exceed 5 % hemolysis in three different concentrations. When red blood cells were exposed to a higher concentration a small percentage was hemolyzed.

The non-hemolytic character at the concentrations range 10–40 μg/mL of lauryl gallate confirms the hemocompatibility, ensuring the protection of drug when encapsulated in superparamagnetic PMMA nanoparticles [9, 38]. In others words, they are similar to the original plasma, which indicates that the superparamagnetic polymeric nanoparticles did not have obvious activation or coagulation factors and thrombin generation [44]. Lastly, superparamagnetic PMMA nanoparticles surface modified with FA provides protection to the drug (lauryl gallate), decreasing toxic effects in non-tumor cells with potential application for controlled intravenous delivery of lauryl gallate.

### 4.3 In vitro cytotoxicity and cellular uptake

Cytotoxicity assays of lauryl gallate on HeLa cells showed that the FA adsorption on the nanoparticles surface promoted a higher reduction in cell viability than free lauryl gallate and nanoparticles without FA. These results can be related with an increase in cellular uptake, due to the interaction of FA with the folate receptor overexpressed on the surface of HeLa cells [25, 60, 61]. Based on the results of cytotoxicity and cellular uptake assays, confocal microscopy and flow cytometry analysis were carried out, as can be seen in Fig. 8. All assays performed corroborate with cytotoxicity assays, in which a higher uptake cellular was observed when the lauryl gallate loaded in superparamagnetic PMMA nanoparticles surface modified with FA was incubated at 37 °C. When the nanoparticles were incubated at 4 °C, assuming that the energy-dependent pathways are inhibited, the nanoparticles were not able to diffuse at 4 °C, suggesting that the nanoparticles were uptake by some energy-dependent pathways [62–64]. Lastly, our results suggest that the higher cellular uptake observed by confocal microscopy and flow cytometry of lauryl gallate loaded in superparamagnetic PMMA nanoparticles surface modified with FA were delivered into HeLa cells via folate receptor-*mediated endocytosis*.

## 5 Conclusion

The synthesis by miniemulsion polymerization of lauryl gallate loaded in superparamagnetic PMMA nanoparticles with the surface modified with FA resulted in a polymeric system with superparamagnetic behavior, excellent colloidal stability, and high EE. The release profile of lauryl gallate showed an initial burst effect, followed by a slow and sustained release, indicating a biphasic release system. The lauryl gallate loaded in superparamagnetic PMMA nanoparticles did not present any cytotoxic effect on non-tumoral cells (L929 and human red blood cells). However, free lauryl gallate presented cytotoxicity in both cells, suggesting that the polymeric system protected against possible toxic effects. Cytotoxicity and cellular uptake studies on HeLa cells showed that lauryl gallate loaded in superparamagnetic PMMA nanoparticles covered by FA was much more efficient than lauryl gallate loaded in superparamagnetic PMMA nanoparticles without FA and free lauryl gallate, suggesting that those nanoparticles were targeted to HeLa cells by folate receptor-mediated endocytosis. Lastly, our studies demonstrated that these superparamagnetic polymeric systems could be an excellent alternative in cancer treatment with targeted drug delivery and controlled release of encapsulated drugs.

**Acknowledgments** The authors thank the financial support from CNPq (Conselho Nacional de Desenvolvimento Científico e Tecnológico), CAPES (Coordenação de Aperfeiçoamento de Pessoal de Nível Superior), and TEM analysis from Laboratório Central de Microscopia Eletrônica of Federal University of Santa Catarina (LCME/UFSC).

**Compliance with ethical standards**

**Conflict of interest** The authors declare that they have no conflict of interest.

## References

1. Huang HS, Hainfeld JF. Intravenous magnetic nanoparticle cancer hyperthermia. Int J Nanomedicine. 2013;8:2521–32.
2. Chertok B, Moffat BA, David AE, Yu F, Bergemann C, Ross BD, Yang VC. Iron oxide nanoparticles as a drug delivery vehicle for MRI monitored magnetic targeting of brain tumors. Biomaterials. 2012;29:487–96.
3. Gupta AK, Gupta M. Synthesis and surface engineering of iron oxide nanoparticles for biomedical applications. Biomaterials. 2005;25:3995–4021.
4. Feuser PE, Bubniak LS, Silva MCS, Cas Viegas A, Castilho-Fernandes A, Nele M, Ricci-Júnior E, Tedesco AC, Sayer C, Araújo PHH. Encapsulation of magnetic nanoparticles in poly(methyl methacrylate) by miniemulsion and evaluation of hyperthemia in U87MG cells. Eur Polym J. 2015;68:355–65.
5. Feuser PE, Castilho-Fernandes A, Nele M, Cas Viegas A, Tedesco AC, Ricci-Júnior E, Sayer C, Araújo PHH. Simultaneous encapsulation of magnetic nanoparticles and zinc phthalocyanine in poly(methyl methacrylate) nanoparticles by miniemulsion polymerization and in vitro studies. Colloid Surf B: Biointerfaces. 2015;135:357–64.
6. Jeon H, Kim J, Lee YM, Kim J, Choi HW, Lee J, Park H, Kang Y, Kim I-S. Poly-paclitaxel/cyclodextrin-SPION nano-assembly for

magnetically guided drug delivery system. J Control Release. 2016;231:68–76.
7. Li Z, Liu S, Wang S, Qiang L, Yang T, Wang H, Möhwald H, Cui X. Synthesis of folic acid functionalized redox-responsive magnetic proteinous microcapsules for targeted drug delivery. J Colloid Interface Sci. 2015;450:325–31.
8. Kumar CSSR, Mohamad F. Magnetic nanomaterials for hyperthermia-based therapy and controlled drug release. Adv Drug Deliver Rev. 2011;63(9):789–808.
9. Huang HS, Hainfeld JF. Intravenous magnetic nanoparticle cancer hyperthermia. Int J Nanomedicine. 2013;8:2521–32.
10. Xu C, Su S. New forms of superparamagnetic nanoparticles for biomedical applications. Adv Drug Deliver Rev. 2013;65:732–43.
11. Mody VV, Cox A, Shah S, Singh A, Bevins W, Parihar H. Magnetic nanoparticle drug delivery systems for targeting tumor. Appl Nanoscience. 2014;4:385–92.
12. Chertok B, Moffat BA, David AE, Yu F, Bergemann C, Ross BD, Yang VC. Iron oxide nanoparticles as a drug delivery vehicle for MRI monitored magnetic targeting of brain tumors. Biomaterials. 2012;29:487–96.
13. Landfester K, Mailander V. Nanocapsules with specific targeting and release properties using miniemulsion polymerization. Exp Opin Drug Deliver. 2013;10:593–609.
14. Chiaradia V, Valério A, Feuser PE, Oliveira D, Araújo PHH, Sayer C. Incorporation of superparamagnetic nanoparticles into poly(urea-urethane) nanoparticles by step growth interfacial polymerization in miniemulsion. Colloids Surf A. 2015;482 (5):596–603.
15. Liu X, Guan Y, Liu H. Surface modification and characterization of magnetic polymer nanospheres prepared by miniemulsion polymerization. Langmuir. 2004;20:10278–82.
16. Shi Z, Guo R, Li W, Zhang Y, Xue W, Tang Y, Zhang Y. Nanoparticles of deoxycholic acid, polyethylene glycol and folic acid-modified chitosan for targeted delivery of doxorubicin. J Mater Sci: Mater Med. 2014;25(3):723–31.
17. Feuser PE, Jacques AV, Carpio JM, Rocha MEM, Silva MCS, Sayer C, Araújo PHH. Superparamagnetic poly(methyl methacrylate) nanoparticles surface modified with folic acid presenting cell uptake mediated by endocytosis. J Nanopart Res. 2016; 18:104.
18. Sahu SK, Mallick SK, Santra S, Maiti TK, Ghosh SK, Pramanik P. In vitro evaluation of folic acid modified carboxymethyl chitosan nanoparticles loaded with doxorubicin for targeted delivery. J Mater Sci: Mater Med. 2010;21:1587–97.
19. Sahoo B, Sanjana K, Devi P, Banerjee R, Maiti TK, Pramanik P, Dhara D. Thermal and pH responsive polymer-tethered multifunctional magnetic nanoparticles for targeted delivery of anticancer drug. ACS Appl Mater Interfaces. 2013;5:3884–93.
20. Mohapatra S, Mallick SK, Kmaiti T, Ghosh SK, Pramanik P. Synthesis of highly stable folic acid conjugated magnetite nanoparticles for targeting cancer cells. Nanotechnology. 2007; 18:385102.
21. Ji Z, Lin G, Meng L, Shen X, Dong L, Fu C, Zhang X. Targeted therapy of SMMC-7721 liver cancer in vitro and in vivo with carbon nanotubes based drug delivery system. J Colloid Interface Sci. 2012;365:143–9.
22. Saltan N, Kutlu HM, Hur D, Izcan A, Ridvan S. Interaction of cancer cells with magnetic nanoparticles modified by methacrylamido-folic acid. Int J Nanomedicine. 2011;6:477–84.
23. Andhariya N, Upadhyay R, Mehta R, Chudasama B. Folic acid conjugated magnetic drug delivery system for controlled release of doxorubicin. J Nanop Res. 2013;15:1416–9.
24. Chen D, Tang Q, Li X, Zhou X, Zang J, Xue W-Q, Xiang J-Y, Guo C-Q. Biocompatibility of magnetic Fe3 O4 nanoparticles and their cytotoxic effect on MCF-7 cells. J Nanomedicine. 2012; 7:4973–85.
25. Lapina VA, Vorobey AV, Pavich TA, Opitz JJ. Targeting diamond nanoparticles into folate-receptor expressing HeLa cells. Appl Spectrosc. 2013;80:414–8.
26. Pala K, Servotka A, Jelen F, Jackimowics P, Otlewski J. Tumor-specific hyphertermia with aptamer-tagget superparamagnetic nanoparticles. Int J Nanomedicine. 2014;9:67–76.
27. Ow Y-Y, Stupans T. Gallic acid and gallic acid derivatives: effects on drug metabolizing enzymes. Curr Drug Met. 2003;4(3):241–8.
28. Klein E, Weber NJJ. In vitro test for the effectiveness of antioxidants as inhibitors of thiyl radical-induced reactions with unsaturated fatty acids. Agr Food Chem. 2001;49:1224–7.
29. Grundhofer P, Niemetz R, Schilling G, Gross GG. Biosynthesis and subcellular distribution of hydrolyzable tannins. Phytochemistry. 2001;57(6):915–27.
30. Zhao B, Gu M. Gallic acid reduces cell viability, proliferation, invasion and angiogenesis in human cervical cancer cells. Oncol Lett. 2013;6(6):1749–55.
31. Manna SK, Kuo MT. Overexpression of glutamylcysteine synthetase suppresses tumor necrosis factor induced apopotosis and activation of nuclear transcription factor B and activator protein. Oncogene. 1999;18:4371–82.
32. Locatelli C, Filippin-Monteiro FB, Creczynski-Pasa TB. Alkyl esters of gallic acid as anticancer agents: a review. Europ J Med Chem. 2013;60:233–9.
33. Stella B, Arpiccoa A, Roccoa F, Marsaud V, Renoirb J-M, Cattel L, Couvreur P. Encapsulation of gemcitabine lipophilic derivatives into polycyanoacrylate nanospheres and nanocapsules. Int J Pharmac. 2007;344:71–7.
34. Ximenes VF, Lopes MG, Nio MSP, Regasini LC, Silva DHS, Fonseca LM. Inhibitory effect of gallic acid and its esters on 2,2′-azobis(2-amidinopropane)hydrochloride (AAPH)-induced hemolysis and depletion of intracellular glutathione in erythrocytes. J Agr Food Chem. 2010;58:5355–62.
35. Alves ACS, Mainardes RM, Khalil NM. Nanoencapsulation of gallic acid and evaluation of its cytotoxicity and antioxidant activity. Mat Sci Eng C-Biomin. 2016;60:126–34.
36. Danhier F, Feron B, Préat V. To exploit the tumor microenvironment: passive and active tumor targeting of nanocarriers for anti-cancer drug delivery. J Control Release. 2010;148:135–6.
37. Gupta AK, Curtis ASG. Surface modified superparamagnetic nanoparticles for drug delivery: interaction studies with human fibroblasts in culture. J Mater Sci: Mater Med. 2004;15(4):493–6.
38. Siafaka P, Betsiou M, Tsolou A, Angelou E, Agianian B, Koffa M, Chaitidou S, Karavas E, Avgoustakis K, Bikiaris D. Synthesis of folate-pegylated polyester nanoparticles encapsulating ixabepilone for targeting folate receptor overexpressing breast cancer cells. J Mater Sci: Mater Med. 2015;26(12):1–14.
39. Costa P, Lobo JMS. Modeling and comparison of dissolution profiles. Euro J Pharm Sci. 2001;13:123–33.
40. International Organization for Standardization (ISO) Biological evaluation of medical devices - Part 5: Tests for in vitro cytotoxicity. 3rd edition. 2009. ISO 10993-5.
41. Zheng W, Gao F, Gu HJ. Magnetic polymer nanospheres with high and uniform magnetite content. J Magn Magn Mater. 2005;288:403–10.
42. Pasanphan W, Chirachanchai S. Conjugation of gallic acid onto chitosan: an approach for green and water-based antioxidant. Carbohydr Polym. 2008;7:169–77.
43. Gao F, Cai Y, Zhou J, Xie X, Ouyang W, Zhang Y, Wang X, Zhang X, Wang X, Zhao L, Tang J. Pullulan acetate coated magnetite nanoparticles for hyperthermia: preparation, characterization and in vitro experiments. Nano Res. 2010;3:23–31.
44. Serrano A, Palacios C, Roy G, Cespon C, Villar ML, Nocito M, Gonzalez-Porqué P. Derivatives of gallic acid induce apoptosis in tumoral cell lines and inhibit lymphocyte proliferation. Arch Biochem Biophys. 1998;350:49–54.

45. He C, Hu Y, Yin L, Tang C, Yin C. Effects of particle size and surface charge on cellular uptake and biodistribution of polymeric nanoparticles. Biomaterials. 2010;31(13):3657–66.
46. Lekshmi MD, Kishore GPN, Reddy PN. In vitro characterization and in vivo toxicity study of repaglinide loaded poly(methyl methacrylate) nanoparticles. Int J Pharm. 2010;396(1-2): 194–203.
47. Yang H, Li Y, Li T, Xu M, Chen Y, Wu C, Dang X, Liu Y. Multifunctional core/shell nanoparticles cross-linked polyetherimide-folic acid as efficient Notch-1 siRNA Carrier for targeted killing of breast cancer. Sci Rep. 2014;4:7072.
48. Dong S, Cho HJ, Lee YW, Roman M. Synthesis and cellular uptake of folic acid-conjugated cellulose nanocrystals for cancer targeting. Biomacromolecules. 2014;15:1560–7.
49. Li R, Feng F, Wang Y, Yang X, Yang X, Yang VC. Folic acid-conjugated pH/temperature/redox multi-stimuli responsive polymer microspheres for delivery of anti-cancer drug. J Colloid Interface Sci. 2014;429:34–44.
50. Ramires LP, Landfester K. Magnetic polystyrene nanoparticles with a high magnetite content obtained by miniemulsion processes. Macromol Chem Physic. 2003;204:22–31.
51. Lima E, De Biasi E, Vasquez Mansilla M, Saleta ME, Effenberg F, Rossi LM, Cohen R, Rechenberg HR, Zysler RD. Surface effects in the magnetic properties of crystalline 3 nm ferrite nanoparticles chemically synthesized. J Appl Phys. 2010; 108:103919.
52. Lima Junior E, Vargas JM, Rechenberg HR, Zysler RD. Interparticle interactions effects on the magnetic order in surface of Fe(3)O(4) nanoparticles. J Nanosci Nantechnol. 2008;8(11): 5913–20.
53. Nowicka AM, Kowalczyk A, Jarzebinska A, Donten M, Krysinski P, Stojek Z. Progress in targeting tumor cells by using drug-magnetic nanoparticles conjugate. Biomacromolecules. 2013;14:828–33.
54. Li C, Wang Z-H, Yu D-G, Williams GR. Tunable biphasic drug release from ethyl cellulose nanofibers fabricated using a modified coaxial electrospinning process. Nanoscale Res Letters. 2014;9(1): 258–77.
55. Yu DG, Wang X, Li XY, Chian W, Li Y, Liao YZ. Electrospun biphasic drug release polyvinylpyrrolidone/ethyl cellulose core/sheath nanofibers. Acta Biomater. 2013;9:5665–72.
56. Huang X, Brazel CS. On the importance and mechanisms of burst release in matrix-controlled drug delivery systems. J Control Release. 2001;73:121–6.
57. Gao P, Nie X, Zou M, Shi Y, Cheng G. Recent advances in materials for extended-release antibiotic delivery system. J Antibiotics. 2011;64:625–34.
58. Fu Y, Kao WJ. Drug release kinetics and transport mechanisms of non-degradable and degradable polymeric delivery systems. Expert Opin Drug Deliv. 2010;7(4):429–44.
59. Rao JP, Geckeler KE. Polymer nanoparticles: preparation techniques and size-control parameters. Prog Polym Sci. 2011; 36(7):887–913.
60. Zhou Q, Zhang Z, Chen T, Guo X, Xhou S. Preparation and characterization of thermosensitive pluronic F127-b-poly(ε-caprolactone) mixed micelles. Colloid Surf B: Biointerfaces. 2011;86(1):45–7.
61. Sabharanjak S, Mayor S. Folate receptor endocytosis and trafficking. Adv Drug Deliver Rev. 2004;8:1099–109.
62. Wibowo SA, Singha M, Reedera KM, Cartera JJ, Kovacha AR, Menga W, Ratnamb M, Zhanga F, Iiia CED. Structures of human folate receptors reveal biological trafficking states and diversity in folate and antifolate recognition. Proc Natl Acad Sci. 2013;110 (38):15180–8.
63. Trindade ES, Bouças RI, Rocha HAO, Dominato J, Paredes-Gamero EJ, Franco CRC, Oliver C, Jamur MC, Dietrich CP, Nader HB. Internalization and degradation of heparin is not required for stimulus of heparan sulfate proteoglycan synthesis. J Cell Physiol. 2008;217(2):360–6.
64. Panariti A, Miserocchi G, Rivolta I. The effect of nanoparticle uptake on cellular behavior: disrupting or enabling functions? Nanotechnol Sci Appl. 2012;5:87–100.